RSC Advances

PAPER

View Article Online
View Journal | View Issue

Cite this: *RSC Adv.*, 2022, **12**, 30650

Influence of TiCN addition on the microstructures and mechanical properties of the AZ31 alloy

Qi-feng Li,[ab] Wei Qiu,[*ab] Wen Xie,[ab] Wei-ying Huang,[ab] Li-bo Zhou,[ab] Yan-jie Ren,[ab] Jian Chen,[ab] Mao-hai Yao,[c] Ai-hu Xiong[c] and Wei Chen[*ab]

Received 23rd August 2022
Accepted 13th October 2022

DOI: 10.1039/d2ra05280f

rsc.li/rsc-advances

The microstructure and mechanical properties of extruded AZ31 + *x*TiCN (*x* = 0, 0.4, 0.8, 1.2 wt%) were investigated, and the strengthening mechanism was discussed. X-ray diffraction and energy dispersive spectroscopy (EDS) confirmed that the Al_4C_3 and Al_2MgC_2 duplex phase particles were generated *in situ* by TiCN and Al particles, which act as the nucleation precursors of Mg grains during solidification. The grain size decreased and then increased with increasing TiCN addition. The yield strength (YS) and ultimate tensile strength (UTS) increased with increasing TiCN addition reaching a maximum (217.5 MPa) at 0.4 wt%, and in contrast, the elongation index (EI) continuously decreased with increasing TiCN addition.

1. Introduction

Magnesium (Mg) alloy is an attractive and promising structural engineering alloy, because of its advantages like light weight, good castability and abundant deposits in the earth.[1,2] However, the low strength, creep resistance and poor machinability of magnesium alloys hinder their further application.[3,4] According to the classical Hall–Petch relationship, grain refinement has been proved to be an effective method to improve the strength of metal materials.[5,6] Moreover, during the refining process, the distribution of the second phase in the Mg–Al alloy is more uniform, which can improve the strength, elongation and reduce the segregation of castings.[8–12] Therefore, various grain refinement methods for Mg–Al based alloys have been developed.

Generally, the grain refinement methods during the casting process of magnesium alloy can be divided into two types: melt treatment and metal alloying.[19,20] Metal alloying is a common refinement method during the liquid forming process in magnesium alloys, which includes solute element and compound particle methods. Solute elements added to magnesium alloys usually have high *Q* value, such as Ti, Zr, Ca, Si, *etc.* It can provide rapid development of constitutional supercooling (CS) to restrict the grain growth.[7] Therefore, some particles like TiB_2,[13–15] AlB_2,[13,16] and AlN[17,18] with good heterogeneous nucleation ability are widely applied for refining process. In addition, the compound can also be added to refine grain size because they can react with certain elements of the alloy *in situ* to form the particle with potentially heterogeneous nucleation capabilities.[13–18] For example, Qiu, *et al.*[19] reported that the addition of 0.5 wt% VN reduces the grain size of AZ31 alloy. Duplex phases composed of AlN and VN can act as nucleation substrates during solidification of α-Mg.

Although the solute paradigm is considered to be the most important factor controlling the grain refinement process, some findings attribute it to the role of the presence of effective heterogeneous nucleation sites in the melt. Among potent nucleants, carbon inoculation is widely employed because of its lower treatment temperature and less fading. So far, many carbonaceous agents have been used as refiners in Mg–Al alloys, such as $MgCO_3$,[22] SiC,[23,24] Al_4C_3,[20,25] particles. There are also other particles, such as TiC[26] and B_2C,[27] which are usually added to magnesium alloys in the form of Al–Ti–C and Al–B–C master alloys. For example, Liu *et al.*[21] discovered that the addition of 1.8 wt% Mg-50% Al_4C_3 master alloy into AZ91D alloy could reduce the grain size from 360 μm to 154 μm.

For the refinement mechanism in Mg–Al base alloys with carbon addition, researchers are mainly focused on determining the role of carbon in grain refinement. According to the edge-to-edge matching crystallographic model,[28] the *d*-value mismatch between the matching directions, should be less than 10%. Recently, a new refinement mechanism was proposed by Huang *et al.*[29] A ternary carbide Al_2MgC_2 was found in the Mg-3% Al alloy inoculated by carbon or SiC powder, and it was believed that Al_2MgC_2 particles can act as a nucleation substrate for α-Mg, leading to alloy refinement. In addition, TiCN and magnesium matrix have the crystallographic orientation relationships by the edge-to-edge matching (E2EM).[30] The calculations show that there exist two possible ORs between α-Mg and TiCN. $[1120]_{Mg}//[110]_{TiCN}$, $(10\bar{1}1)Mg//(111)_{TiCN}$ and $[1120]_{Mg}//$

[a]*School of Energy and Power Engineering, Changsha University of Science & Technology, Changsha, Hunan 410114, China. E-mail: yekyek2009@126.com; weichen@csust.edu.cn*

[b]*Key Laboratory of Energy Efficiency and Clean Utilization, The Education Department of Hunan Province, Changsha University of Science & Technology, Changsha, Hunan 410114, China*

[c]*Hunan Rare Earth Metal Material Research Institute, Institute of Rare Earth Light Alloys, Changsha, 410126, China*

$[110]_{TiCN}$, $(0002)_{Mg}//(111)_{TiCN}$.[31] Recent studies have shown that small amounts of TiCN nanoparticles dispersed into the matrix by high-energy sonication can effectively refine pure aluminum,[32] Al–Cu[33] and Al–Si alloys.[34–36] Chen *et al.*[37] added $TiC_{0.7}N_{0.3}$ nanoparticles to Al–20Bi alloys, and as a result, the size of the Bi phase was reduced from 821 μm to 7.5 μm.

Unfortunately, there is no report about nano-TiCN powder reinforced AZ31 alloy. In this paper, the microstructure evolution and strengthening mechanism of x wt% TiCN ($x = 0$, 0.4, 0.8, 1.2) in AZ31 extruded alloy were comparative studied. The effect of TiCN nanopowder addition on the growth behavior of α-Mg grains was discussed from the heterogeneous nucleation and solute restriction theory.

2. Experimental procedure

According to the designed nominal composition, in a ZG-25 vacuum medium frequency melting furnace with mixed gas (CO_2 + SF_6), electromagnetic stirring was carried out for 15 min at about 750 °C and held for 10 min before pouring into graphite mold; AZ31 + x wt% TiCN cast alloy ($x = 0$, 0.4, 0.8, 1.2) was prepared. In order to eliminate intracrystalline segregation and improve microstructure heterogeneity, the ingot was heated at 400 for 20 h.

Samples for optical microscope (OM, Zeiss 200 MAT) observation were ground with 400–2000 grit SiC papers, and subsequently polished with 0.5 mm diamond paste and then etched in a solution of 1 ml nitric acid, 1 ml acetic acid, 1 ml oxalic acid and 97 ml distilled water. Fig. 1 presents the typical microstructures of the AZ31 alloys refined with different amounts of TiCN. For AZ31 alloy without TiCN, the grains are coarse, and the average grain size is about 132.8 μm. With the addition of TiCN increased to 0.4 wt% and 0.8 wt%, the average grain size decreased to 77.6 μm and 85.8 μm, respectively. However, when the TiCN content increased from 0.8 wt% to 1.2 wt%, the grain size showed an obvious coarsening trend, and the average grain size increased from 85.8 μm to 127 μm.

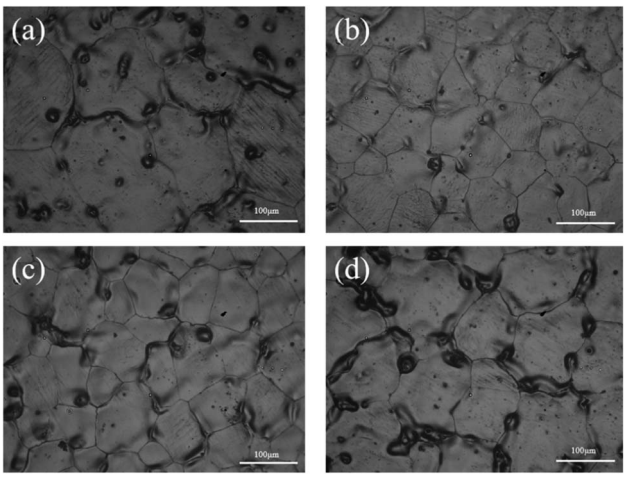

Fig. 1 Microstructures of AZ31 alloys refined by different amounts of TiCN: (a) 0% TiCN; (b) 0.4% $MgCO_3$; (c) 0.8% $MgCO_3$; (d) 1.2% $MgCO_3$.

The extrusion experiments were completed on a horizontal extruder with temperature of 400 °C and ratio of 16. Microstructure analysis was observed by scanning electron microscopy (SEM, FEI Quanta 250) equipped with energy dispersive spectroscopy (EDS). The phase composition was identified by X-ray diffraction (XRD) with a scanning angle from 10° to 90° and a scanning rate of 5° min^{-1}. The test instrument used in the uniaxial tensile test of this experiment is the new Sansi CMT-5105 microcomputer-controlled electronic universal testing machine. The test parameters are uniform uniaxial tension at room temperature at a rate of 1 mm s^{-1}. The size of the tensile specimen was determined according to the standard ASTM E8. The specific shape and parameters are shown in Fig. 2.

3. Results and discussion

3.1. Phases and microstructures in the extruded AZ31 alloy

Fig. 3 shows the SEM microstructure images of the surface of AZ31 + x wt% TiCN. There are a large number of fine particles in the alloy with TiCN. After TiCN particles are added to the alloy, these second phases are partially agglomerated in the extrusion band and some are distributed at grain boundaries, as shown in Fig. 3(c), where the particles are mostly fine.

After adding TiCN particles to the alloy, it can be seen that there is an obvious un-dynamically recrystallized (Un-DRXed) region in the alloy, especially when the TiCN content reaches 1.2 wt%, there are large-size un-DRXed grains (Fig. 3c and d). It suggested that the addition of TiCN particles hinders the dynamic recrystallization of the extruded AZ31 magnesium alloy. These particles are broken during the hot extrusion process, and are concentrated on the extrusion band. In addition, a large number of fine particles appear in the alloys with TiCN addition (Fig. 3c), and these particles are uniformly distributed in the particle area, and the grain size around the particle aggregation area is smaller than that in the region without particles. In order to determine the composition of these particles, the energy dispersive spectrum (EDS) of the particles in the marker area A in Fig. 3c was obtained. The results are shown in Table 1, which shows that these particles are mainly composed of Mg, Al and C, and these particles are mainly Al_4C_3 or Al_2MgC_2.

In order to explore the composition of the second phase in the extruded alloy with the addition of refiner, XRD was performed. Fig. 4 shows the XRD results of the AZ31 alloys with and without TiCN addition. As shown in Fig. 4, all the alloys mainly consisted of α-Mg and Al_8Mn_5 phases. Furthermore, adding 0.4 wt% TiCN to the AZ31 alloy did not cause the formation of any new phases, which is possibly related to the low contents of TiCN. However, after adding 0.8 wt% and 1.2 wt% TiCN to the

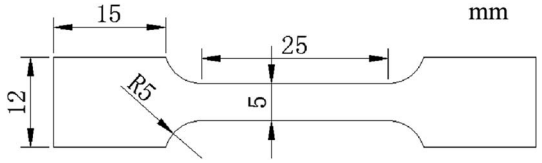

Fig. 2 Diagram of a tensile specimen.

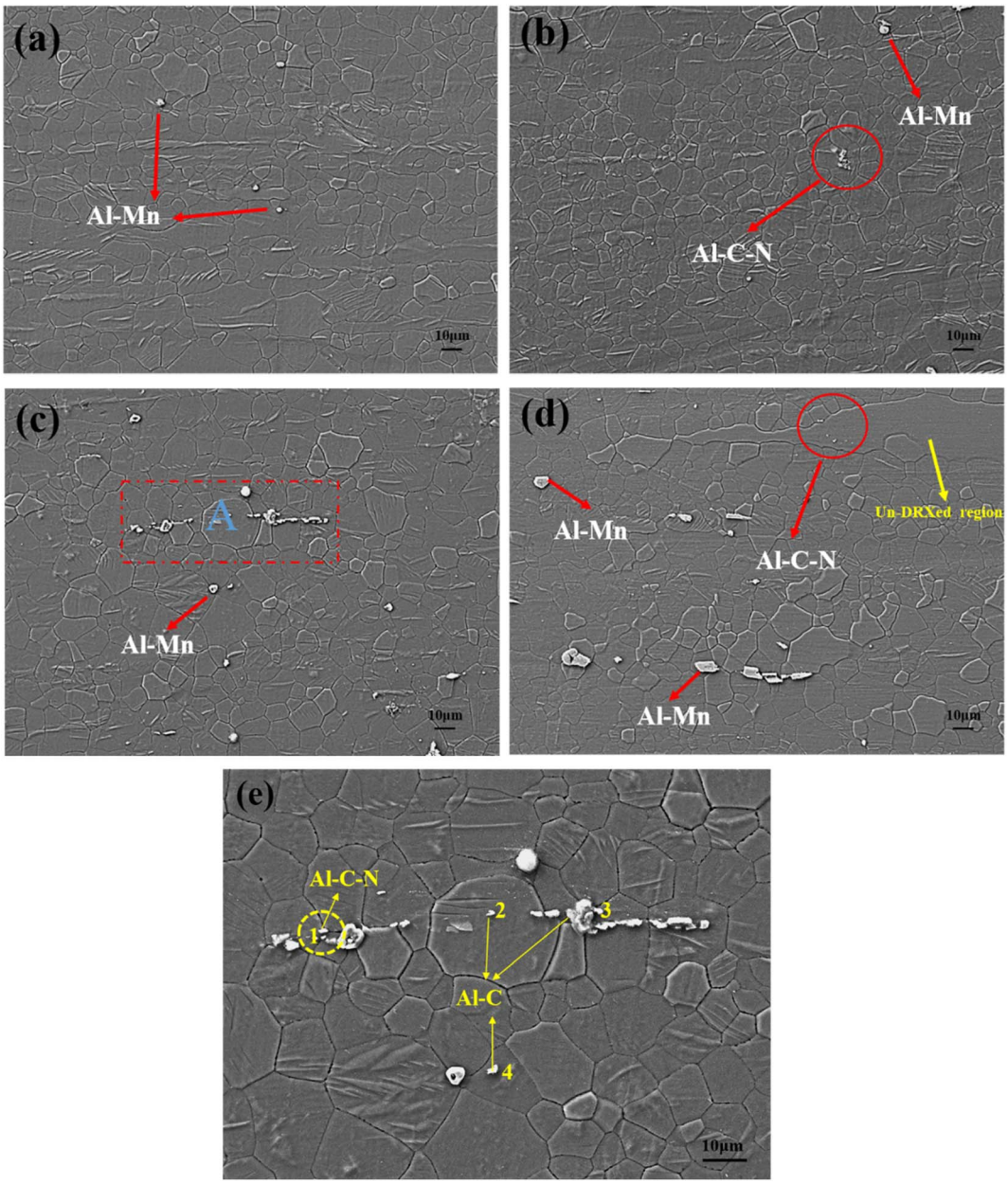

Fig. 3 SEM microstructure of surface of the extruded alloy; (a–d) AZ31 + x wt% TiCN (x = 0, 0.4, 0.8, 1.2). (e) A region enlargement diagram.

AZ31 alloy, the Al_4C_3 new phase formed in the alloys. The following figure can be found that the diffraction peaks of the extruded state alloy of AZ31 with the addition of TiCN are shifted somewhat overall, with the addition of TiCN powder, the (006) peak of Al_4C_3 shifts to a higher angle and the intensity of the Al_4C_3 peak increases with the increase in C content; the ' N' of TiCN reacts with the matrix to produce the AlN phase. Due to the low content, the (100) peak of AlN was only detected in the AZ31 alloy with 1.2 wt% TiCN.

Table 1 EDS analysis results of particles in region A in Fig. 3 (at%)

	1	2	3	4
Mg	41.37	50.52	60.67	60.32
Al	35.54	24.91	25.80	23.73
Zn	0.04	0.17	0.34	0.26
Mn	0.43	1.28	0.06	0.13
C	20.09	23.10	13.11	15.31
N	2.53	0	0	0
Ti	0	0.02	0.01	0

Fig. 5 shows the average grain size of AZ31 alloy with and without TiCN. The grain size of the original extruded AZ31 alloy is mainly concentrated in 5 ~ 7 μm. After adding 0.4 wt% TiCN, the average grain size is 4.92 μm. When the TiCN content is 0.8 wt%, the average grain size is 5.09 μm. When the TiCN content reaches 1.2 wt%, the grain size of extruded alloy is 6.07 μm. The grain size of the extruded alloy is the smallest when the TiCN content is 0.4 wt%. In summary, after adding TiCN particles with different contents, the grain size decreases with different degrees.

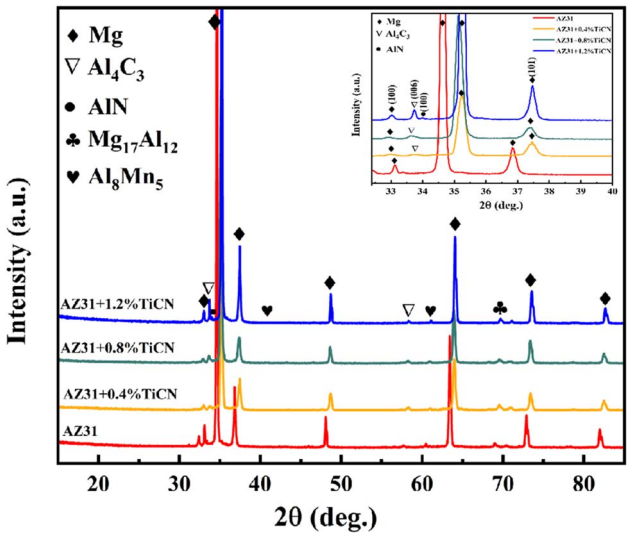

Fig. 4 XRD patterns of AZ31 magnesium alloy extruded with different TiCN contents.

3.2. Mechanical properties and fracture analysis

Fig. 6 shows the engineering stress–strain curves of as-extruded magnesium alloy AZ31 + x wt% TiCN (x = 0, 0.4, 0.8, 1.2) at room temperature and the variation of yield strength (YS), ultimate tensile strength (UTS) and elongation (EI) with TiCN content.

It can be seen from Fig. 6 that the YS, UTS and EI of the original extruded AZ31 magnesium alloy are 155.2 MPa, 268.5 MPa and 14.8%, respectively. After adding 0.4 wt% TiCN, the YS, UTS and EI of the extruded alloy are 217.5 MPa, 293.3 MPa and 13.7%, respectively, which the YS and UTS increased by 40% and 9.2%, and the EI decreased slightly. After 0.8 wt% TiCN was added, the YS, UTS and EI of the extruded alloy are 171.5 MPa, 268 MPa and 12.4%, respectively. When the addition of TiCN reaches 1.2 wt%, the YS, UTS and EI of the extruded alloy are 171.2 MPa, 268.7 MPa and 8.3%, respectively. The plasticity decreases by 43.9% compared with that of the original extruded alloy.

In summary, the YS and UTS of the extruded alloy after adding TiCN particles are higher than those of the original extruded AZ31. It can be seen that the YS and UTS of the extruded alloy are the highest. When the addition is 0.4 wt%. With the increasing of TiCN particle content, the YS and UTS show a downward trend. When the content of TiCN powder increases to 1.2 wt%, the fracture mechanism changes into a mixed mode of intergranular fracture and transgranular fracture. More TiCN powder, due to powder segregation, may produce thick edges, showing brittleness, and easy to crack penetration. The continuous increase of TiCN particles will deteriorate the mechanical properties of the metal, mainly in the reduction of plasticity.

Fig. 7 shows the SEM morphology of the tensile fracture of AZ31 magnesium alloy with different TiCN particles. It can be

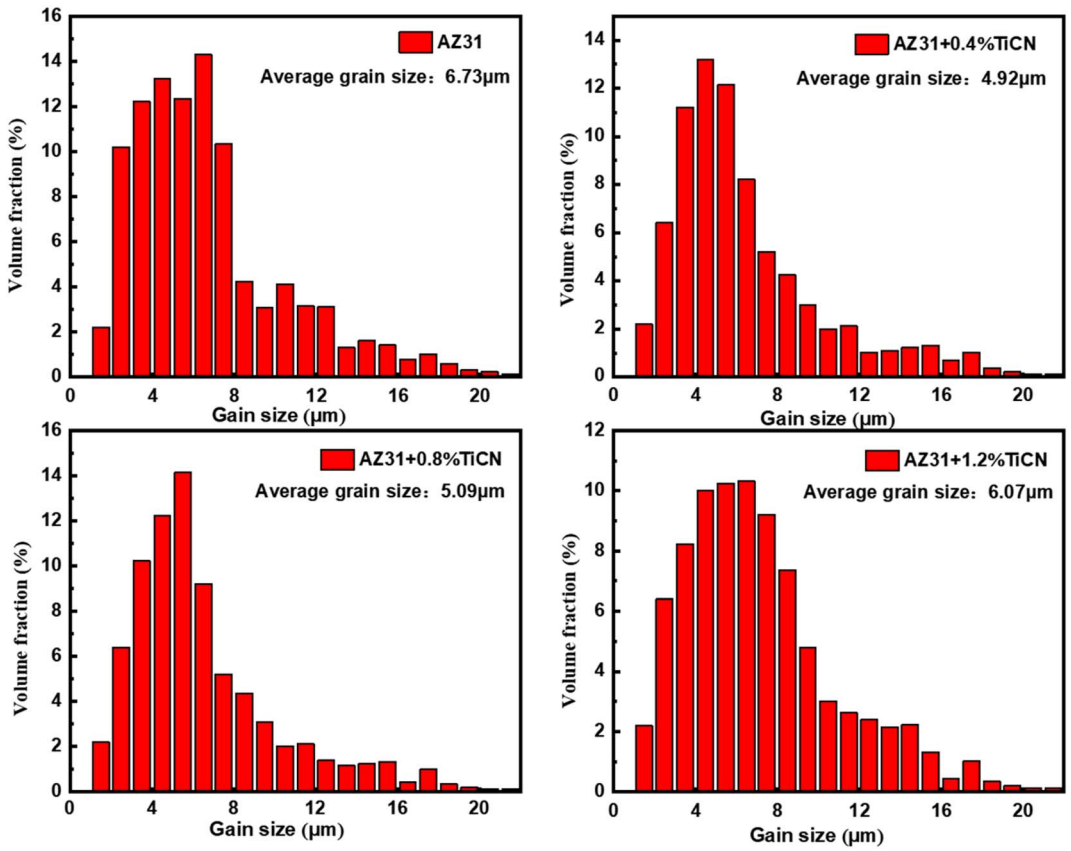

Fig. 5 Effect of TiCN addition rate on average grain size of AZ31 alloy.

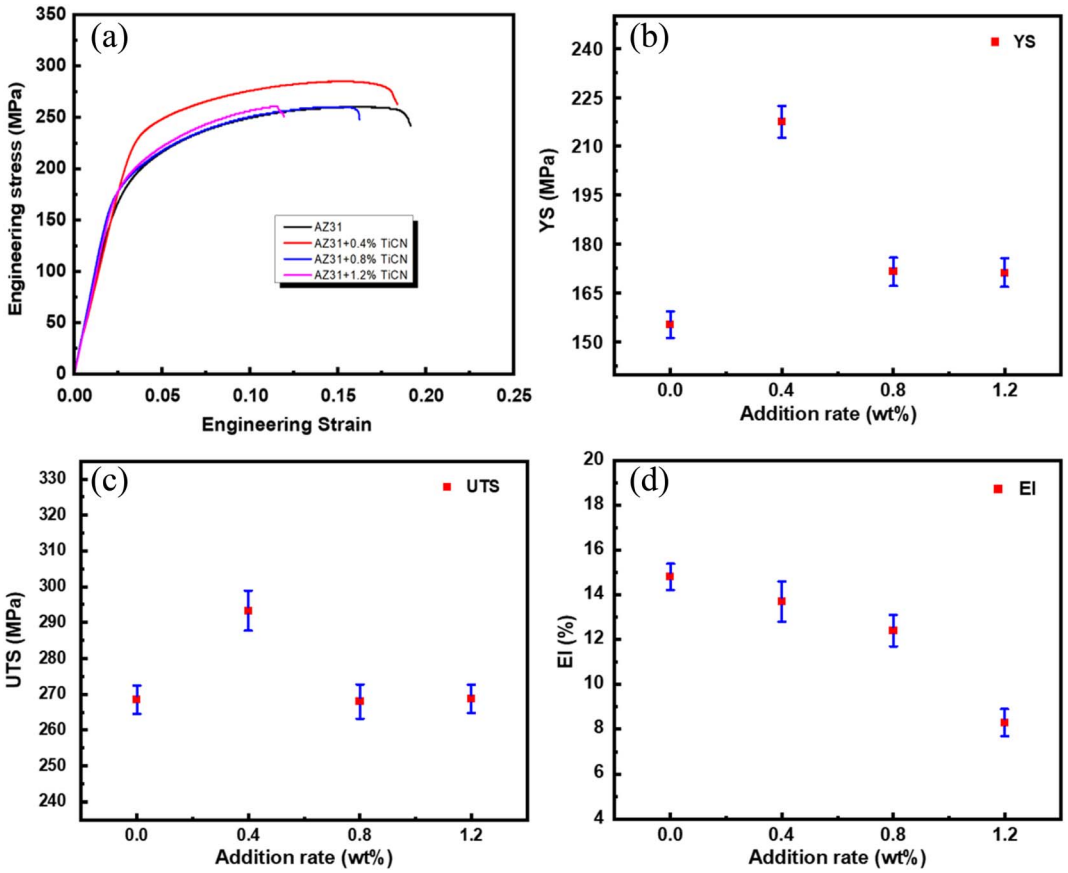

Fig. 6 (a) Engineering stress–strain curve of extruded magnesium alloy AZ31 + *x* wt% TiCN (*x* = 0, 0.4, 0.8, 1.2); (b) yield strength; (c) ultimate tensile strength; (d) elongation.

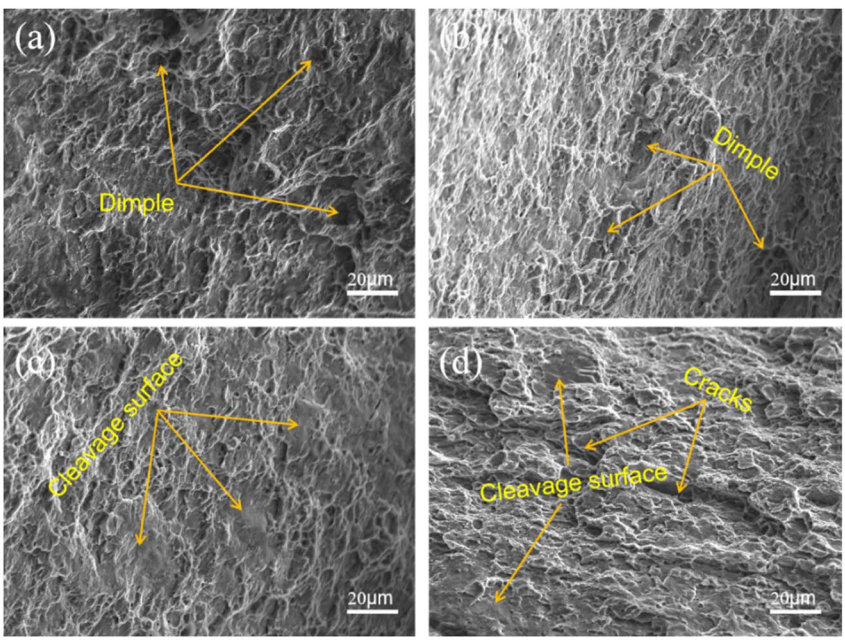

Fig. 7 SEM morphology of tensile section of alloy (a–d) AZ31 + *x* wt% TiCN (*x* = 0, 0.4, 0.8, 1.2).

Table 2 Lattice mismatch of Al_4C_3, Al_2MgC_2 with Mg[24,28]

Particle	Crystallographic	Lattice parameter/nm	Disregistry in close-packed plane/%
Mg	HPC	$a = 0.3203$, $c = 0.52002$	0
Al_4C_3	HPC	$a = 0.3331$, $c = 0.4990$	4.05
Al_2MgC_2	HPC	$a = 0.33797$, $c = 0.5822$	5.32

Table 3 Q value of common solute elements in magnesium alloy[29]

Elements	$Q = m(k-1)$	Elements	$Q = m(k-1)$
Fe	52.26	Sr	3.51
Zr	38.29	Ce	2.74
Ca	11.94	Sc	2.61
Si	9.25	Yb	2.53
Ni	6.13	Y	1.7
Zn	5.31	Sn	1.47
Cu	5.28	Pb	1.03
Ge	4.41	Sb	0.53
Al	4.32	Mn	0.15

seen from Fig. 7(a) that the fracture surface presents a network morphology, such as marked by yellow arrow in the figure, a large number of dimples are distributed on the surface, and there is basically no cleavage surface, which is a typical ductile fracture morphology. Fig. 7(b) also shows the similar morphology as Fig. 7(a), and its surface is distributed with smaller dimples. It can be seen that the magnesium alloy containing 0.4 wt% TiCN should have better plasticity than the original extruded alloy. The fracture morphology of Fig. 7(c) is different. In addition to the local ductile fracture morphology of the dimple, there are also obvious cleavage planes, such as the yellow arrow in the figure. In general, the fracture mode is a combination of ductile fracture and brittle fracture, and the plasticity should be significantly lower than that of alloys without and with 0.4 wt% TiCN. When the TiCN content reaches 1.2 wt%, a large number of cleavage planes and obvious cracks appear on the fractured surface. Its plasticity is the worst, which is consistent with the experimental results in Fig. 6(d).

3.3. Grain refinement mechanism

The common methods of grain refinement include increasing the nucleation rate and inhibiting grain growth. It is generally accepted that the presence of the effective nucleation site in the alloy increases the possibility of nucleation, and the addition of TiCN promoted the grain refinement of the alloy, which is the main factors leading to the strength increase. According to the above experimental analysis, Al_8Mn_5, Al_4C_3 and Al_2MgC_2 particles may be effective nucleation sites for α-Mg. From a crystallographic point of view, previous literature proved that Al_8Mn_5 particles cannot be used as effective nucleation sites for α-Mg.[38] The potential of Al_4C_3 and Al_2MgC_2 as nucleation sites for α-Mg can be demonstrated by crystallography. Table 2 lists the lattice mismatch degrees of Al_4C_3, Al_2MgC_2 and Mg. According to the Bramfitt theoretical model, the particle can act as a heterogeneous shaped nucleation site if the nucleation mismatch is less than 12%.[39] Therefore, both Al_4C_3 and Al_2MgC_2 particles can be used as effective nucleating agents for AZ31 alloy. It is also noteworthy that Al_4C_3 and Al_2MgC_2 can exist simultaneously as nucleation sites. Hard particles Al_4C_3 and Al_2MgC_2 distributed in the matrix may improve tensile properties by promoting dispersion strengthening. Sun *et al.*[40] found that fine and hard intermetallic phases dispersed in the softer α-Mg matrix can prevent dislocation movement and form dislocation buildup, thus improving strength. In addition, the refinement of the β-phase ($Mg_{17}Al_{12}$) in the alloy is also an important factor in improving the mechanical properties. Previous studies[41] have found that in the coarse AZ91D alloy, there are many large pores of the eutectic β-phase between the developed dendrites. As a result, stress concentration tends to develop around these pores, which leads to cracks preferentially appearing and extending, resulting in relatively low UTS.

In the present study, heterogeneous nucleation is not the only factor controlling grain size, the inhibition effect from solute elements also play an important role in alloy refinement. Based on the results of phase analysis in Table 1, it can be assumed that the Ti element in the melt is present in the form of Ti atoms during solidification. In other words, the Ti element is similar to a solute element in the melt. According to the growth inhibition theory of solute elements,[42] a large "growth restriction factor" (GRF) not only means that a large number of solute atoms accumulate at the solid–solution interface during solidification, which limits the growth of grains, but also provides a large nucleation subcooling for the growing crystal, promoting formation of stable nuclei on the nucleating matrix. Wang *et al.*[42] calculated a Q value for Ti of about 5.95×10^4 in the Mg–Ti system, which is several orders of magnitude higher than that of the common elements, as can be seen from Table 3. Therefore, it can be concluded that the element Ti can effectively hinder the growth of α-Mg grains, which leads to the refinement of AZ31 magnesium alloy. However, high content of Ti may lead to the grain coarsening of Mg-based alloys, which explains that when the addition amount of TiCN is 1.2 wt%, the grain size of the alloy becomes larger.

4. Conclusions

(1) TiCN particles were added into AZ31 alloy to achieve remarkable refinement. In AZ31 alloy containing 0.4 wt% TiCN particles, the average grain size from 6.73 μm to 4.92 μm.

(2) After adding TiCN particles, the *in situ* formation of Al_4C_3 and Al_2MgC_2 heterogeneous nucleation is the main reason of grain refinement of magnesium alloy.

(3) The mechanical properties of the TiCN modified AZ31 alloy are improved. The YS and UTS of the alloy with 0.4 wt% TiCN were the best. The YS increases from 155.2 MPa to 217.5 MPa, and the UTS increases from 268.5 MPa to 293.3 MPa.

In contrast, the EI continuously decreased with increasing TiCN addition.

Conflicts of interest

There are no conflicts to declare.

Acknowledgements

The authors gratefully acknowledge the financial supports from the National Natural Science Foundation of China (No. 52171099, 51301025, 51140001), Natural Science Foundation of Hunan Province (No. 2020JJ4610). Changsha University of Science and Technology "Practical Innovation and Entrepreneurship Improvement Program" project (CLSJCX22094).

References

1 E. Karakulak, A review: past, present and future of grain refining of magnesium castings, *J. Magnesium Alloys*, 2019, **7**, 355–369.
2 X. J. Wang, D. K. Xu, R. Z. Wu, X. B. Chen, Q. M. Peng, L. Jin, Y. C. Xin, Z. Q. Zhang, Y. Liu, X. H. Chen, G. Chen, K. K. Deng and H. Y. Wang, What is going on in magnesium alloys, *J. Mater. Sci. Technol.*, 2018, **34**, 245–247.
3 H. Yu, C. Li, Y. Xin, A. Chapuis, X. Huang and Q. Liu, The mechanism for the high dependence of the Hall-Petch slope for twinning slip on texture in Mg alloys, *Acta Mater.*, 2017, **128**, 313–326.
4 U. M. Chaudry, T. H. Kim, S. D. Park, Y. S. Kim, K. Hamad and J. G. Kim, Effects of calcium on the activity of slip systems in AZ31 magnesium alloy, *Mater. Sci. Eng., A*, 2019, **739**, 289–294.
5 T. Han, G. Huang, Q. Deng, G. Wang, B. Jiang, A. Tang, Y. Zhu and F. Pan, Grain refining and mechanical properties of AZ31 alloy processed by accumulated extrusion bonding, *J. Alloys Compd.*, 2018, **745**, 599–608.
6 R. Zheng, T. Bhattacharjee, A. Shibata, T. Sasaki, K. Hono, M. Joshi and N. Tsuji, Simultaneously enhanced strength and ductility of Mg–Zn–Zr–Ca alloy with fully recrystallized ultrafine grained structures, *Scr. Mater.*, 2017, **131**, 1–5.
7 S. M. Fatemi and A. Zarei-Hanzaki, Microband/twin recrystallization during back extrusion of AZ31 magnesium, *Mater. Sci. Eng., A*, 2017, **708**, 230–236.
8 R. Cheng, F. Pan, S. Jiang, C. Li, B. Jiang and X. Jiang, Effect of Sr addition on the grain refinement of AZ31 magnesium alloys, *Prog. Nat. Sci.: Mater. Int.*, 2013, **23**, 7–12.
9 A. Zhang, H. Hao, X. Liu and X. Zhang, Effects of precipitates on grain size and mechanical properties of AZ31-*x*% Nd magnesium alloy, *J. Rare Earths*, 2014, **32**, 451–457.
10 Y. Chen, L. Jin, D. Fang, Y. Song and R. Ye, Effects of calcium, samarium addition on microstructure and mechanical properties of AZ61 magnesium alloy, *J. Rare Earths*, 2015, **33**, 86–92.
11 X. Hu, P. Fu, D. Stjohn, L. Peng, M. Sun and M. Zhang, On grain coarsening and refining of the Mg-3Al alloy by Sm, *J. Alloys Compd.*, 2016, **663**, 387–394.
12 H. Lin, M. Yang, H. Tang and F. Pan, Effect of minor Sc on the microstructure and mechanical properties of AZ91 Magnesium Alloy, *Prog. Nat. Sci.: Mater. Int.*, 2018, **28**, 66–73.
13 Y. Wang, X. Zeng and W. Ding, Effect of Al-4Ti-5B master alloy on the grain refinement of AZ31 magnesium alloy, *Scr. Mater.*, 2006, **54**, 269–273.
14 X. L. Ma, X. Wang, X. L. Li and L. Yang, Effect of Al5Ti1B master alloy on microstructures and properties of AZ61 alloys, *Trans. Nonferrous Met. Soc. China*, 2010, **20**, s397–s401.
15 S. Liu, Y. Zhang, H. Han and B. Li, Effect of Mg-TiB2 master alloy on the grain refinement of AZ91D magnesium alloy, *J. Alloys Compd.*, 2009, **487**, 202–205.
16 M. Suresh, A. Srinivasan, K. R. Ravi, U. T. S. Pillai and B. C. Pai, Influence of boron addition on the grain refinement and mechanical properties of AZ91 Mg alloy, *Mater. Sci. Eng., A*, 2009, **525**, 207–210.
17 H. M. Fu, M. X. Zhang, D. Qiu, P. M. Kelly and J. A. Taylor, Grain refinement by AlN particles in Mg-Al based alloys, *J. Alloys Compd.*, 2009, **478**, 809–812.
18 H. Z. Ye, X. Y. Liu and B. Luan, In situ synthesis of AlN particles in Mg-Al alloy by Mg_3N_2 addition, *Mater. Lett.*, 2004, **58**, 2361–2364.
19 W. Qiu, Z. Liu, R. Yu, J. Chen, Y. Ren, J. He, W. Li and C. Li, Utilization of VN particles for grain refinement and mechanical properties of AZ31 magnesium alloy, *J. Alloys Compd.*, 2019, **781**, 1150–1158.
20 M. Suresh, A. Srinivasan, K. R. Ravi, U. T. S. Pillai and B. C. Pai, Microstructural refinement and tensile properties enhancement of Mg-3Al alloy using charcoal additions, *Mater. Sci. Eng., A*, 2011, **528**, 2502–2508.
21 S. Liu, Y. Chen and H. Han, Grain refinement of AZ91D magnesium alloy by a new Mg-50% Al_4C_3 master alloy, *J. Alloys Compd.*, 2015, **624**, 266–269.
22 J. Du, Z. Yao, S. Han and W. Li, Discussion on grain refining mechanism of AM30 alloy inoculated by $MgCO_3$, *J. Magnesium Alloys*, 2017, **5**, 181–188.
23 T. J. Chen, Y. Ma, W. B. Lv, Y. D. Li and Y. Hao, Grain refinement of AM60B magnesium alloy by SiC particles, *J. Mater. Sci.*, 2010, **45**, 6732–6738.
24 T. J. Chen, X. D. Jiang, Y. Ma, Y. D. Li and Y. Hao, Grain refinement of AZ91D magnesium alloy by SiC, *J. Alloys Compd.*, 2010, **496**, 218–225.
25 S. Nimityongskul, M. Jones, H. Choi, R. Lakes, S. Kou and X. Li, Grain refining mechanisms in Mg-Al alloys with Al_4C_3 microparticles, *Mater. Sci. Eng., A*, 2010, **527**, 2104–2111.
26 X. T. Liu, H. Hao, X. X. Zhu and X. G. Zhang, Grain refining effect of Mg by novel particle cluster-containing Al-Ti-C master alloy, *Trans. Nonferrous Met. Soc. China*, 2015, **25**, 1804–1810.
27 M. Guolong, H. Guang and L. Xiangfa, Grain refining efficiency of a new Al-1B-0.6C master alloy on AZ63 magnesium alloy, *J. Alloys Compd.*, 2010, **491**, 165–169.
28 M. X. Zhang, P. M. Kelly, M. Qian and J. A. Taylor, Crystallography of grain refinement in Mg-Al based alloys, *Acta Mater.*, 2005, **53**, 3261–3270.

29 Y. Huang, K. U. Kainer and N. Hort, Mechanism of grain refinement of Mg-Al alloys by SiC inoculation, *Scr. Mater.*, 2011, **64**, 793–796.
30 M.-X. Zhang, P. Kelly, M. Qian and J. Taylor, Crystallography of grain refinement in Mg–Al based alloys, *Acta Mater.*, 2005, **53**(11), 3261–3270.
31 H. Li, K. Wang, G. Xu, H. Jiang, Q. Wang and W. Ding, Nanoparticle-induced growth behavior of primary α-Mg in AZ91 alloys, *Mater. Des.*, 2020, **196**, 109146.
32 K. Wang, H. Jiang, Q. Wang, B. Ye and W. Ding, A Novel Method to Achieve Grain Refinement in Aluminum, *Metall. Mater. Trans. A*, 2016, **47**, 4788–4794.
33 K. Wang, G. P. Xu, H. Y. Jiang, Q. D. Wang and W. J. Ding, Effects of TiC0.5N0.5 nanoparticles on the microstructure, mechanical and thermal properties of TiC0.5N0.5/Al-Cu nanocomposites, *J. Mater. Res. Technol.*, 2020, **9**(2), 2044–2053.
34 K. Wang, H. Y. Jiang, Y. X. Wang, Q. D. Wang, B. Ye and W. J. Ding, Microstructure and mechanical properties of hypoeutectic Al–Si composite reinforced with TiCN nanoparticles, *Mater. Des.*, 2016, **95**, 545–554.
35 K. Wang, H. Y. Jiang, Y. W. Jia, H. Zhou, Q. D. Wang, B. Ye and W. J. Ding, Nanoparticle- inhibited growth of primary aluminum in Al–10Si alloys, *Acta Mater.*, 2016, **103**, 252–263.
36 K. Wang, H. Y. Jiang, Q. D. Wang and W. J. Ding, Influence of nanoparticles on microstructural evolution and mechanical properties of Sr-modified Al-10Si alloys, *Mater. Sci. Eng. A*, 2016, **666**, 264–268.
37 L.-Y. Chen, J.-Q. Xu, H. Choi, H. Konishi, S. Jin and X.-C. Li, Rapid control of phase growth by nanoparticles, *Nat. Commun.*, 2014, **5**, 3879.
38 Y. Wang, M. Xia, Z. Fan, X. Zhou and G. E. Thompson, The effect of Al_8Mn_5 intermetallic particles on grain size of as-cast Mg-Al-Zn AZ91D alloy, *Intermetallics*, 2010, **18**, 1683–1689.
39 L. Bruce, Bramfitt, The Effect of Carbide and Nitride Additions on the Heterogeneous Nucleation Behavior of Liquid Iron, *Metall. Trans.*, 1970, **1**, 1987–1995.
40 H. F. Sun, C. J. Li and W. Bin Fang, Evolution of microstructure and mechanical properties of Mg-3.0Zn-0.2Ca-0.5Y alloy by extrusion at various temperatures, *J. Mater. Process. Technol.*, 2016, **229**, 633–640.
41 T. J. Chen, Y. Ma, B. Li, Y. D. Li and Y. Hao, Wear behavior of thixoformed AZ91D magnesium alloy: a comparison with permanent mould cast alloy, *Mater. Sci. Eng., A*, 2007, **445–446**, 477–485.
42 Y. Wang, X. Zeng, W. Ding, A. A. Luo and A. K. Sachdev, Grain refinement of AZ31 magnesium alloy by titanium and low-frequency electromagnetic casting, *Metall. Mater. Trans. A*, 2007, **38**, 1358–1366.